Advanced Powder Technology 28 (2017) 3085–3094

Contents lists available at ScienceDirect

Advanced Powder Technology

journal homepage: www.elsevier.com/locate/apt

Original Research Paper

Synthesis of heterogeneous Ag-Cu bimetallic monolith with different mass ratios and their performances for catalysis and antibacterial activity

Manisha Sharma [a], Satyajit Hazra [b], Soumen Basu [a,*]

[a] School of Chemistry and Biochemistry, Thapar University, Patiala, Punjab 147004, India
[b] Saha Institute of Nuclear Physics, Kolkata 700064, India

A R T I C L E   I N F O

Article history:
Received 10 July 2017
Received in revised form 18 September 2017
Accepted 25 September 2017
Available online 9 October 2017

Keywords:
Bimetallic
Silver/copper
Monoliths
Mesoporous
Nitrophenol reduction
Antibacterial activity

A B S T R A C T

Combination of two or more metallic particles along with high surface area and porous structure exhibits enhanced catalytic as well as antibacterial activity. Here, Ag-Cu bimetallic monoliths were synthesized by nanocasting method by strictly adjusting the molar ratio of Ag-Cu. This work is mainly focused on the effect of molar ratio (Ag:Cu) on surface area (14–110 m^2/g) and porous size of bimetallic monoliths, which has great influence on enhancement of catalytic and antimicrobial activity. The catalytic activity of bimetallic Ag-Cu monoliths was evaluated for the reduction of 4-nitrophenol (4-NP) to 4-aminophenol (4-AP) in the presence of excess $NaBH_4$. The reaction rate follows pseudo-first order for reduction of 4-NP with a reduction efficacy of ~95%. The effect of Ag:Cu molar ratio and reaction conditions on the rate of reaction were investigated. In comparison with novel monometallic silver monoliths, bimetallic Ag-Cu monoliths exhibit high catalytic performance on the reduction of 4-NP. These heterogeneous catalysts were effortlessly recovered and reused (up to 8 cycles) after completion of catalytic reaction. As bimetallic Ag-Cu particles are well-known for antibacterial activity, so bactericidal properties of synthesized monoliths are tested against *E. coli* and *B. subtilis* bacteria by minimum inhibitory concentration method (MIC). The calculated EC_{50} (half maximum effective concentration) after completion of incubation period, against *E. coli* and *B. subtilis* were 22.87 ± 0.015 and 23.33 ± 0.09 respectively using Ag/Cu-3 bimetallic monolith.

1. Introduction

Manufacturing of various antipyretic and analgesic drugs requires some strong transitional aromatic compounds. These compounds are also used remarkably as a photographic developer, anticorrosion-lubricant and hair-dyeing agent [1]. Thus, being a standard precursor substance for aromatic amino compounds, a novel and cost-effective process for catalytic reduction of hydrogen of nitro-aromatic compound is always in demand. Also, nitro aromatic compounds (like nitrophenols) are considered as most common organic pollutant in waste water introduced from pesticides, dyes, paper, pharmaceuticals and other chemical industries [2]. Nitrophenols has been considered as most toxic and hazardous pollutants by the US Environmental Protection Agency [3]. For removal of nitrophenols from water, an environment friendly system is required. Consequently, to convert these toxic pollutants into valuable amines, many research has been done on the synthesis of monometallic or bimetallic nanoparticles/nanocomposites [4–8]. Even if metallic particles show good catalytic activity, but their applicability on a large scale was limited due to their high cost. To overcome this problem, bimetallic nanocomposites (two different metals bound to form one composite) are formed either in core-shell structure, alloys or mixture of two metals. Bimetallic nanocomposites are more attractive than individual metallic nanocomposites mostly because of enhanced catalytic properties and they exhibit different thermal, magnetic, electrical and optical properties due to synergistic or fine-tuning effects [9–11]. Bimetallic composites can be synthesized by reduction of two different metal ions at the same time in the presence/absence of surfactant/polymer [12,13] or straight reduction of one metal ion over the nuclei of other metal [14,15]. Based on different synthesis procedures, both alloy or core-shell structures can be synthesized. Some reported bimetallic combinations (like Ag-Cu, Ag-Au, Pd-Pt and Au-Pd) have applications in heterogeneous catalysis, fuel cell electrocatalysis and sensing [16].

* Corresponding author.
E-mail address: soumen.basu@thapar.edu (S. Basu).

https://doi.org/10.1016/j.apt.2017.09.023
0921-8831/

Metallic elements like silver and copper are traditionally well known as bactericidal. The properties of these metal particles get amplified at nanoscale due to high surface area and volume ratio [17,18]. Metallic nanoparticles have a special potential to interact with microbial membrane, due to which they can be used as disinfectants for waste water treatment. Chen et al. have reported the synthesis of Cu-Ag core shell particles by chemical reduction of silver over commercial micrometric Cu particles to study the anti-oxidation and antibacterial properties [19]. Rousse et al. have studied the antibacterial properties of Cu-Ag bimetallic nanopowders using sonochemically synthesized Cu nanoparticles followed by a coating of silver ions [20].

With regard to realistic applications as a catalyst, porous materials became a hot topic for thorough study. Mesoporous metal nanoparticles as a catalyst have the advantage of very high surface area and large pore size distribution, which help in mass transfer and increase in a number of active sites on the surface of nanomaterial. For catalytic function, numerous promising procedures can be used to synthesize mesoporous materials. Even though numerous papers have been published on synthesis of noble mesoporous metal composites, but hardly some are focused on bimetallic mesoporous monoliths like sliver with copper due to difficult and complex approach needed for the synthesis [21–23].

In this work, synthesis of mesoporous Ag-Cu bimetallic monoliths with a varying molar ratio of Cu has been reported using previously synthesized silver monoliths. Synthesized porous Ag-Cu monoliths have been used as a heterogeneous catalyst to study the catalytic reduction of the nitroaromatic (4-NP) compound. Adding up to this, antibacterial activity against both gram positive and negative bacteria was also studied by minimal inhibitory concentration (MIC) using bimetallic monoliths.

2. Materials

Silver nitrate, ammonia (28–30%), cupric nitrate, nitric acid (69%), sodium hydroxide and sodium borohydride were purchased from Merck. Polyethylene glycol (MW 35,000 g/mol) and cetyltrimethyl ammonium bromide were purchased from Sigma Aldrich. Tetraethoxysilane and 4-nitrophenol (4-NP) were purchased from Alfa Aesar. All the chemicals and reagents used in this study are of analytical grade and used without further purification.

2.1. Preparation of Ag-Cu monolith

The detailed procedure for the synthesis of silver monolith has been discussed in our previous paper [24]. Cupric nitrate was used as precursor for Ag-Cu monolith synthesis. Cupric nitrate sol (in different molar ratios, which is defined in Table 1) along with a 0.1 M $NaBH_4$ was impregnated into silver monoliths in the presence of nitrogen atmosphere. Later, wet impregnated monoliths were dried for 10 h at 80 °C with a heating rate of 1 °C/min. Impregnation procedure was repeated for at least five times to get homogeneous impregnation of cupric solution into the pore of silver monoliths and to get solid Ag-Cu monoliths. At the time of drying, oxidation of Cu may result in the formation of Cu_2O in a little amount on monolithic surface which is confirmed by UV–Vis spectroscopy and XRD analysis. Afterwards, composites of Ag-Cu monoliths were finally calcined at 200 °C for 6 h at the heating ramp of 1 °C/min.

2.2. Instrumentations

X-ray diffraction analysis (XRD) was analyzed using Pan Analytical (X'Pert-pro) diffractometer using Cu Kα radiation (λ = 1.5406 Å). The sample morphology and elemental analysis were studied by FESEM and EDS by Hitachi SU 8010 field emission scanning electron microscope operating at 30 kV. Detailed structural analysis of bimetallic nature of Ag-Cu monolith was done using a high-resolution transmission electron microscope (HRTEM) (FEI TECHNAI-G2 operating at 200 kV). The oxidation state of Ag-Cu monolith was determined from PHI 5200 mode X-ray photo- electron spectroscopy (XPS) system. Surface area and pore-size distributions were evaluated through Brunauer–Emmett–Teller (BET) method and Barrett–Joyner–Halenda (BJH) model by using BELSORP MINI-II (Bel, Japan) surface area and pore size analyzer. Before each set of measurements, samples were degassed at 200 °C in vacuum for more than 3 h. The excitation of 4-NP and kinetic parameters were stately studied using a Champion UV- 500 spectrophotometer.

2.3. Antibacterial studies

The antimicrobial activity of synthesized mesoporous Ag-Cu bimetallic monolith (with varying molar ratio) was evaluated by minimum inhibitory concentration (MIC) method against *E. coli* (MTCC-77) and *B. subtilis* (MTCC-441). Luria broth (LB) was taken as a medium for growing and preserving the bacterial liquid cultures. 10 ml of bacterial culture was developed from a single colony. 5 ml of LB was used to inoculate the bacterial cells in glass test tubes. Different Ag-Cu bimetallic monoliths (0–660 μg) was added to the bacterial culture and the cultures were transferred to the incubator with constant agitation (130 rpm) for 24 h at 37 °C (under aerobic conditions). Optical density of bacterial culture was noted at 600 nm after completion of action. The outcomes were drew by mean of 3 mutually independent experiments. EC_{50} (half maximum effective concentration), was also determined to measure the concentration of bimetallic monolith required to attain the 50% reduction in bacterial growth.

2.4. Catalytic reduction of nitro compound

A catalytic stability and activity of heterogeneous Ag-Cu bimetallic catalyst was evaluated for reduction process of 4-NP. The standard procedure for reduction reaction as used by Pradhan et al. [25] was performed in a quartz cuvette (3 ml). Initially, 200 μL of 0.1 M freshly prepared $NaBH_4$ solution was mixed to a solution containing 30 μL of 0.01 M 4-NP and 2 mL of deionized water. The reaction process does not start at all without addition of catalyst. But with the addition of catalyst, it drives to accomplish to conversion 4-AP. The solution was mixed by frail shaking after addition of catalyst and excitation of 4-NP was investigated by UV–Vis spectrophotometer.

Table 1
Textural properties of Ag-Cu monoliths.

Monolith	Ratio (Ag:Cu)	S_{BET} ($m^2\ g^{-1}$)	Mesopore diameter (nm)	Micropore diameter (nm)	Mesopore volume ($cm^3\ g^{-1}$)	Micropore volume ($cm^3\ g^{-1}$)
Ag/Cu-0	1:0	14 ± 5	25.06	–	0.04	–
Ag/Cu-1	1:0.5	39 ± 5	21.2	1.2	0.27	0.038
Ag/Cu-2	1:0.75	52 ± 5	12.4	1	0.13	0.055
Ag/Cu-3	1:1	110 ± 5	8.3	1.3	0.25	0.050

3. Results and discussion

3.1. Structural characterizations

According to IUPAC classification, all samples exhibited typical type – IV adsorption isotherm (Fig. 1a). Table 1 displayed the textural properties of Ag-Cu monoliths (with different molar ratios) determined by N_2–physisorption. The specific surface area of Ag-Cu monoliths regularly increases with the enhancement in molar ratio of Cu metal ions, which were calculated through multipoint BET equation. The data of pore size distribution specifies that Ag-Cu monoliths were mostly mesoporous in nature along with a small number of micropores as shown in Fig. 1b.

The UV–Visible spectra for Ag-Cu bimetallic monolith with the different molar ratio (Fig. 2a) showed a change in an absorption spectrum throughout the emergence of monometallic to the bimetallic monolith. It is confirmed from literature, the peak at 424 nm was validated for Ag whereas peak at ~800 nm can be validated to Cu_2O [26,27], which forms due to oxidation of Cu while heating/drying of Ag-Cu monoliths. Although no blue or red shift was observed with the change in the molar ratio of Cu ions change in intensity was noticed. In an attempt to check the crystalline nature of the synthesized bimetallic Ag–Cu monoliths (with different molar ratio), XRD analysis was carried out. Fig. 2b clearly identify the crystal planes for both Cu and Ag. As shown in XRD pattern, three main characteristic diffraction peaks at 2θ = 38.22, 44.34 and 64.36 corresponding to (1 1 1), (2 0 0) and (2 2 0) crystal planes of face-centered cubic (fcc) phase for silver is observed (JCPDS card no. 4-783). Two characteristic diffraction peaks at 2θ 42.29 and 50.13 corresponding to (1 1 1) and (2 0 0) crystal planes of fcc phase for copper are observed (JCPDS card no. 4-836). A small peak of Cu_2O (1 1 1) was also found with an increment of Cu molar ratio indicating a little oxidation of Cu. Surface micrographs (by SEM analysis) of Ag-Cu monoliths with different molar ratio are shown in Fig. 3. It can observe that the surface morphology and roughness of all samples are almost alike. But the pore size of all the monoliths are different which can be correlated through BJH pore distribution curve. It is also analyzed that with the increase of Cu molar ratio, surface area becomes high because, with the impregnation of nanoparticles, micropores get developed on monolithic system. Further, EDS with elemental mapping was used to confirm the bimetallic structure and the distribution of Ag/Cu-3 monolith. Fig. 4 shows the atoms of Ag and Cu have a homogeneous distribution. To find the elemental composition and oxidation states of

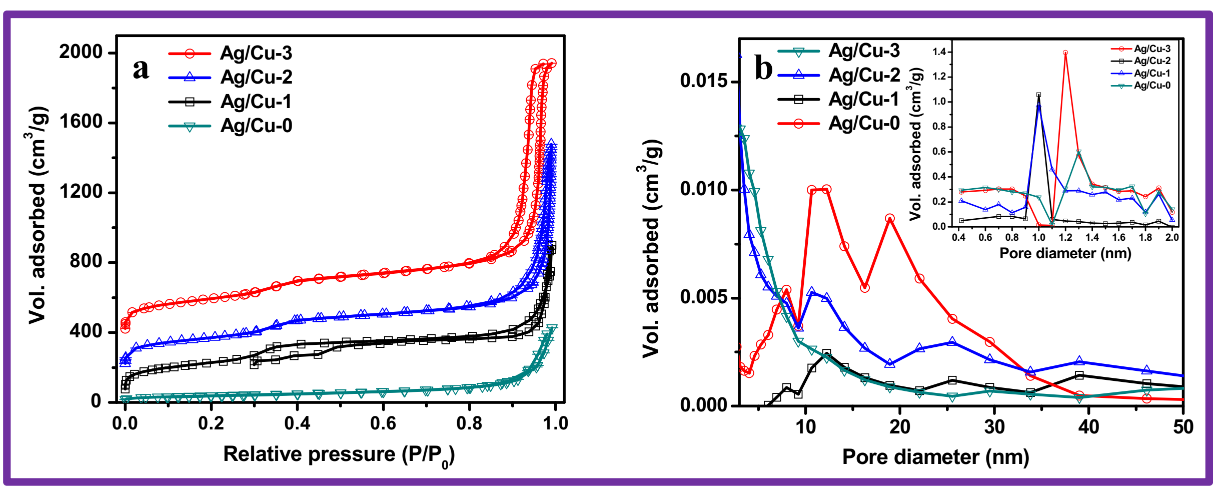

Fig. 1. (a) N_2 adsorption desorption isotherm and (b) mesopore distribution curves through BJH plot (inset contains micropore distribution curves through MP plot) for Ag/Cu monoliths with different molar ratios.

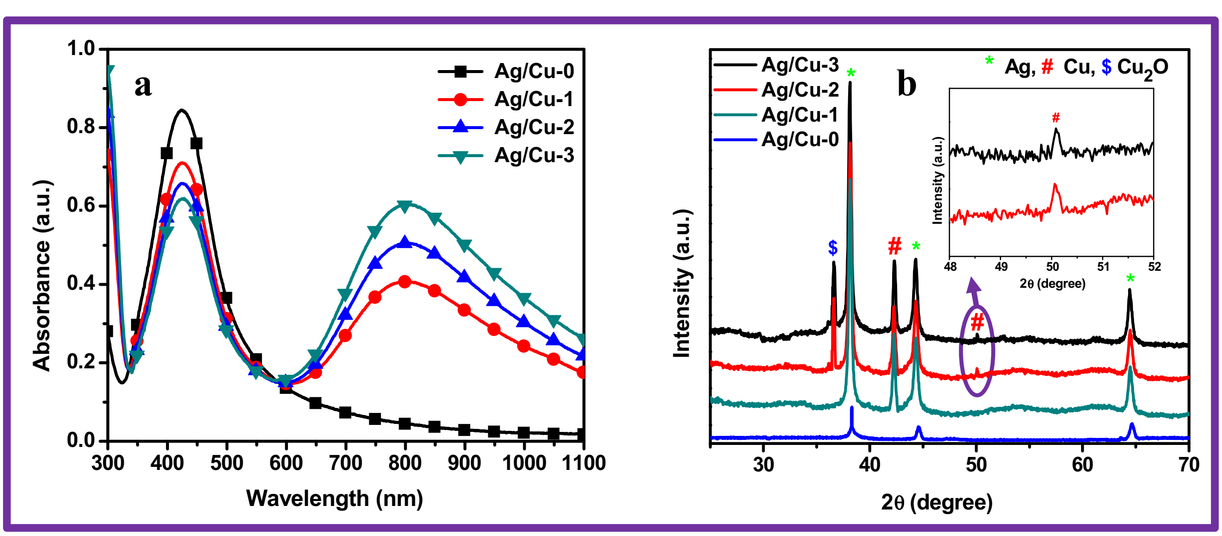

Fig. 2. (a) UV–visible spectra and (b) XRD pattern of Ag/Cu monoliths with different molar ratios.

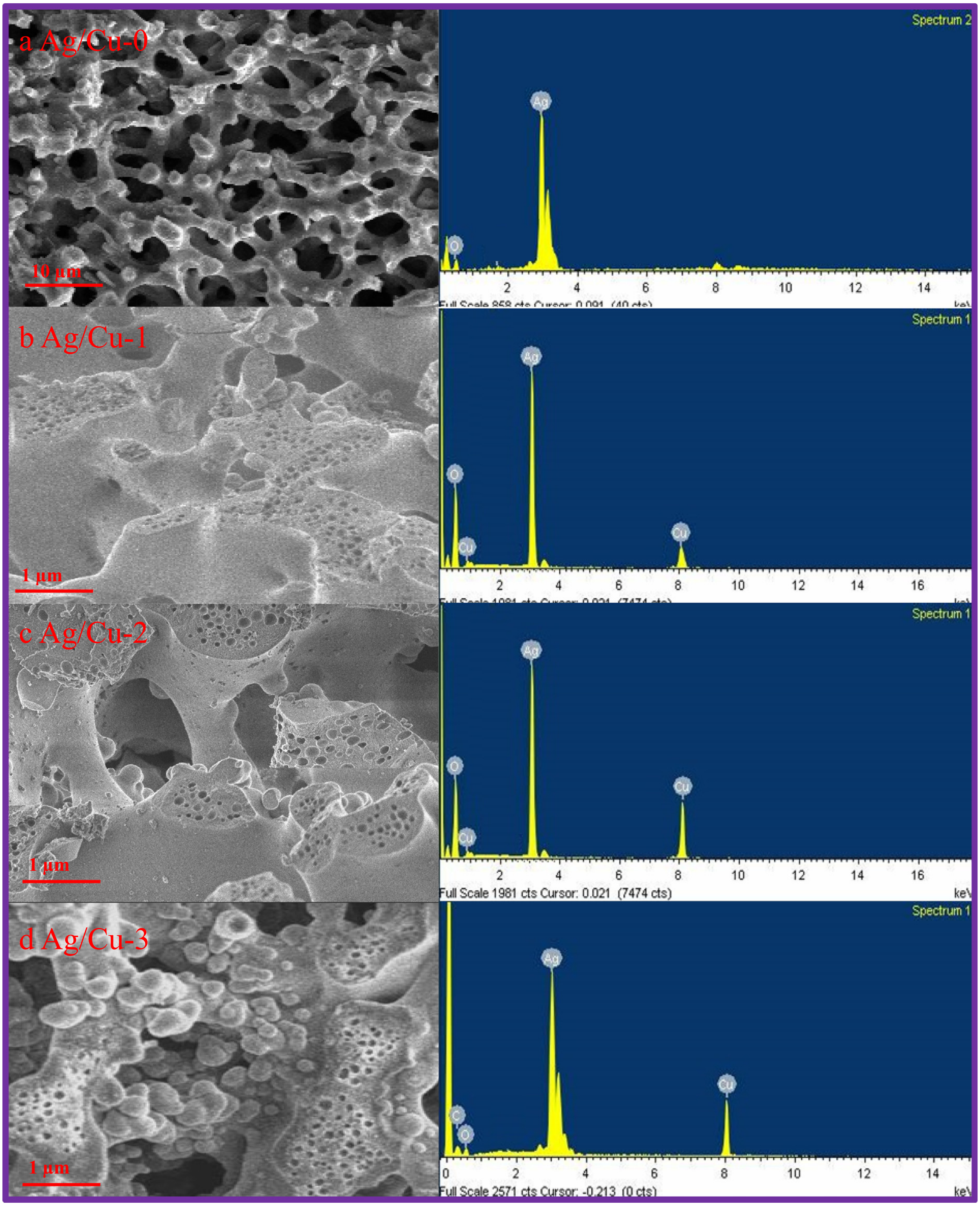

Fig. 3. SEM images and EDX spectrum for Ag/Cu monoliths with different molar ratios.

Ag-Cu monolith, XPS of Ag/Cu-3 was performed. The XPS spectra showing the presence of Ag, Cu and O elemental composition in Fig. 5a. The core level of zero valent Ag confirmed by binding energy values of two peaks, Ag3$d_{5/2}$ (367.6 eV) and Ag3$d_{3/2}$ (373.2 eV), as shown in Fig. 5b. Moreover, no traces of oxidation of Ag are measured due to the good symmetry and peak position. In the core level of Cu2p, two strong peaks for Cu2$p_{3/2}$ (932.3 eV) and Cu2$p_{1/2}$ (952.5 eV) associated with zero-valent Cu are observed (Fig. 5c). Yet, most of the Cu present in Cu(0) state, slight shake-up lines are also observed due to Cu_2O at peak of 943.1 eV. So, a little amount of oxidation of Cu can be predicted which can be reliable with XRD. Besides, the peak of O1$s_{1/2}$ with binding energy 531.7 eV corresponding to zero-valent O (Fig. 5d) may be the result of the adsorption of O from the atmosphere at the time of heat treatment. TEM analysis was performed to investigate about the core shell structure formation in synthesized bimetallic monoliths. Fig. 6(a and b) shows the core shell nature of Ag/Cu-3 monoliths having core diameter of 25 nm along with 3.7 nm of

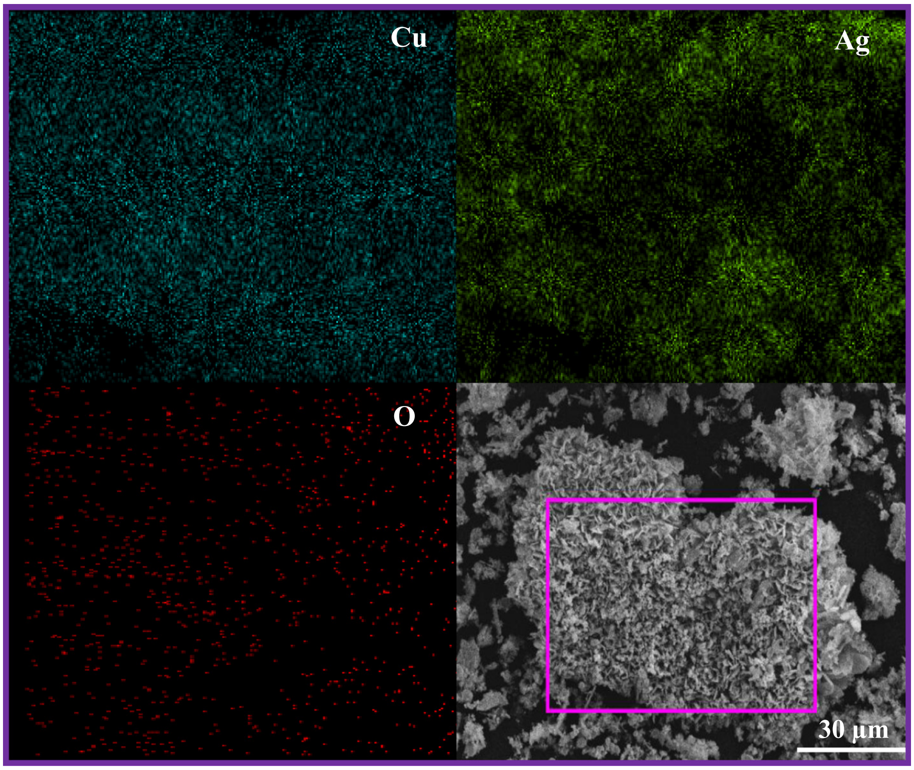

Fig. 4. SEM-EDS elemental mapping of Ag/Cu-3 bimetallic monolith.

Cu shell. A fascinating thing is that in a single shell, a few of Cu encapsulates more than one Ag particles. Fig. 6c shows the selected area electron diffraction (SAED) pattern of Ag/Cu-3 monoliths. SAED pattern supports the formation of bimetallic Ag-Cu monolith and confirms the fcc crystallite planes for Ag and Cu. HRTEM image presenting interface between Ag and Cu has been shown in Fig. 6d.

3.2. Antimicrobial activity

Silver and copper have been known as an antibacterial agent over decades. Due to low cytotoxicity and known antibacterial properties, researcher's interest has been renewed to work on silver and copper nanoparticle synthesis. The antibacterial effect of metallic nanoparticles has been widely studied but the mechanism behind the action has not been interpreted fully. Maximum studies have emphasized that a direct contact between nanoparticles and bacteria results in bacterial cell-wall or membrane rupture and the ruptured cell wall permits the diffusion of nanoparticles inside the bacteria which enhance the changes in biomolecules. Metallic nanoparticles have an antibacterial effect because of continuous release of generation of an oxidative stress by reactive oxygen species (ROS). Silver ions generate ROS and copper induces hydroxyl radicals which help them to rupture both DNA and proteins present in bacteria [20]. Recently, many researchers started working on the synthesis of specific bimetallic nanoparticles (in core shell arrangement) with great chemical stability, very little cytotoxicity and long-term effect. Due to the core shell arrangement chance of oxidation of copper/silver is reduced. Here, in this work, in an attempt to explore the antibacterial performances of Ag-Cu bimetallic monoliths against *E. coli* and *B. subtilis*, a constant amount (0–660 μg) Ag-Cu bimetallic monolith was added to 5 ml of LB culture of bacteria. Fig. 7 shows the plot for percentage growth of bacteria (both *E. coli* and *B. subtilis*) vs. concentration of Ag-Cu bimetallic monolith. The measured EC_{50} (half maximum effective concentration) values of bimetallic monolith have been shown in Table 2.

3.3. Catalytic activity

We are observant to the fact that water pollution by phenolic compounds is of massive anxiety. Among them, nitrophenols have been considered as most rebellious and toxic pollutant which occurs in paper and pharmaceutical industrial wastewater. Bimodal porous nature of synthesized monoliths fascinates us to explore their catalytic effect from the point of abatement of water pollution. Initially, the freshly prepared $NaBH_4$ solution was added to a solution containing 4-NP and water mixture. The reduction process does not start at all but the clear yellow color solution of 4-NP changes into greenish yellow color with the addition of $NaBH_4$, this change is the resultant of increase in alkalinity (pH 9–10) of the solution, due to this 4-NP transforms into nitrophenolate ions which remain stable if no catalyst is added. An instant change in color was observed after addition of a catalyst in the solution and this change also recommends a shift in the absorbance bands. Fig. 8(a and b) shows the UV–Vis spectra presenting the decrease in the main peak for nitrophenolate ions at λ_{max} = 400 nm along with generation of another peak at λ_{max} = 295 nm indicating generation of 4-AP. The establishment of perfect isosbestic points at λ_{max} = 265 nm and 317 nm specifies that 4-AP is the only product formed. Generally, the 4-NP reduction reaction follows first-order rate law kinetic model in order to quantify the reaction kinetics. Hence, the apparent reaction rate constant k values with respect to all synthesized catalysts were calculated from a linear plot between ln (C_t/C_0) and time (s) as shown in Fig. 8c and the rate constant (k) can be calculated according to Eq. (1)

$$k = \frac{1}{t} \ln \frac{C_t}{C_0} \quad (1)$$

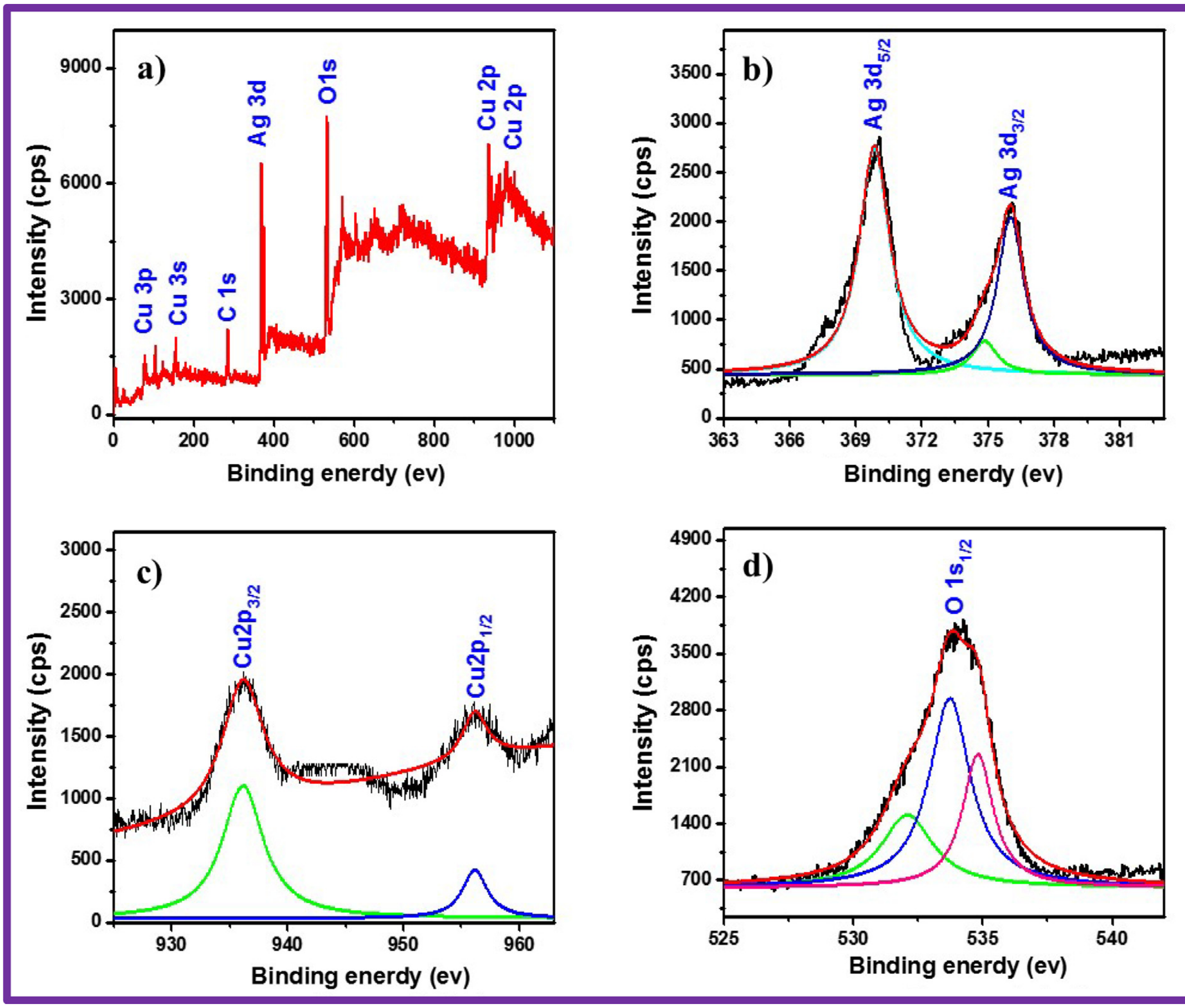

Fig. 5. (a) XPS spectra, (b) Ag 3d core level spectra, (c) Cu 2p core level spectra and (d) O 1s core level spectra for Ag/Cu-3 bimetallic monolith.

where C_0 and C_t are the initial and final concentration of 4-NP at the time (t) respectively. Table 3 displays the apparent rate constant calculated from the logarithmic plot for all samples. The catalytic activity and reduction rate follows in the order of Ag/Cu-3 > Ag/Cu-2 > Ag/Cu-1 > Ag/Cu-0. Due to the synergistic electronic effect, bimetallic composites have high electron density on the surface by means of electron transfer from one metallic state to other. When 4-NP interacts with Ag and Cu, bonding and antibonding interaction occur as a result of overlapping between adsorbate state and metal state. Moreover, bimetallic composites have stronger binding energy as compared to monometallic particles and attributed to strong binding energy bimetallic composites has faster reaction rate constant [28,29]. Besides, high surface area and number of active sites are considered as other factors for the enhanced catalytic performance of Ag/Cu-3 monoliths.

Here, a thought must be paid to a fact that, in all cases, no induction period (delay time t_0) was noticed and the reduction started immediately after addition of a catalyst in the reaction mixture. This induction period is supposed to be the time needed for activation of catalyst in the reaction mixture or for $NaBH_4$ to eliminate surface oxides on the catalyst. This is an opposite behavior to the other reported literature by some groups [30,31]. In this case, hydrogen ions liberated from $NaBH_4$ purged out the air and stops the oxidation of 4-AP as all reactions were carried out in atmospheric conditions. Development of small bubbles on the surface of the catalyst after addition of $NaBH_4$ helps in mixing of the solution and provides optimum conditions for regular reaction to take place.

Amount of catalyst used for catalytic reduction also has a significant effect in controlling the rate of the reaction and to quantify this effect, amount of catalyst was altered keeping rest of the parameters constant. The rate of the reduction reaction escalates with a simultaneous increase in catalyst amount. Rate vs. amount of catalyst plot is shown in Fig. 8d. Also, a connection between the concentration of either 4-NP or $NaBH_4$ and rate constant was acknowledged. Although keeping rest of the parameters constant, increase in the concentration of 4-NP resulted in a decrement in rate constant was observed (Fig. 9a) because the high concentration of 4-NP fully occupied most of the surface of the catalyst and slow downs the reaction whereas an increase in concentration of $NaBH_4$ results in escalation of rate (Fig. 9b). This report concludes that only H^- ions get absorbed and with more concentration of H^- ions on the surface of catalyst leads to enhancement of the rate of reaction. But, above 500 μl concentration of $NaBH_4$ almost constant rate is observed due to the competitive adsorption of both 4-NP and $NaBH_4$ on the surface of Ag-Cu monoliths. Similar findings were detected by other research groups [5,32,33].

3.3.1. Turnover frequency

For evaluating the catalytic efficiency of heterogeneous Ag-Cu monoliths, turnover number (TON) and turnover frequency (TOF) can be used [34]. TON is characteristically defined as the total

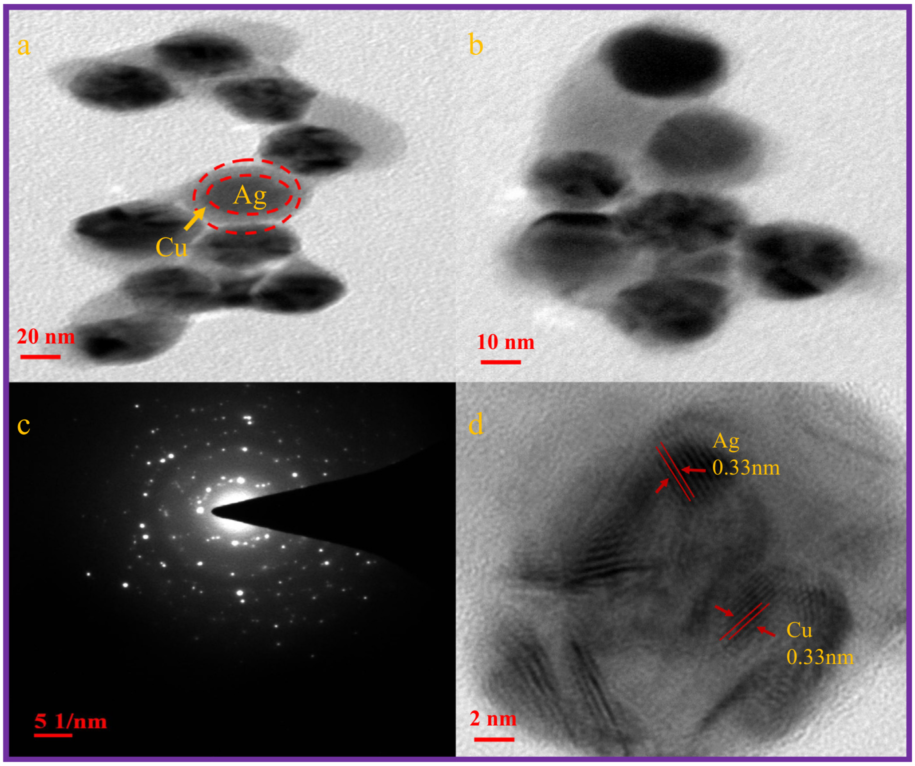

Fig. 6. HRTEM images of Ag/Cu-3 bimetallic monolith with (a) low, (b) high magnifications, (c) SAED pattern and (d) HRTEM image showing interface between Ag and Cu.

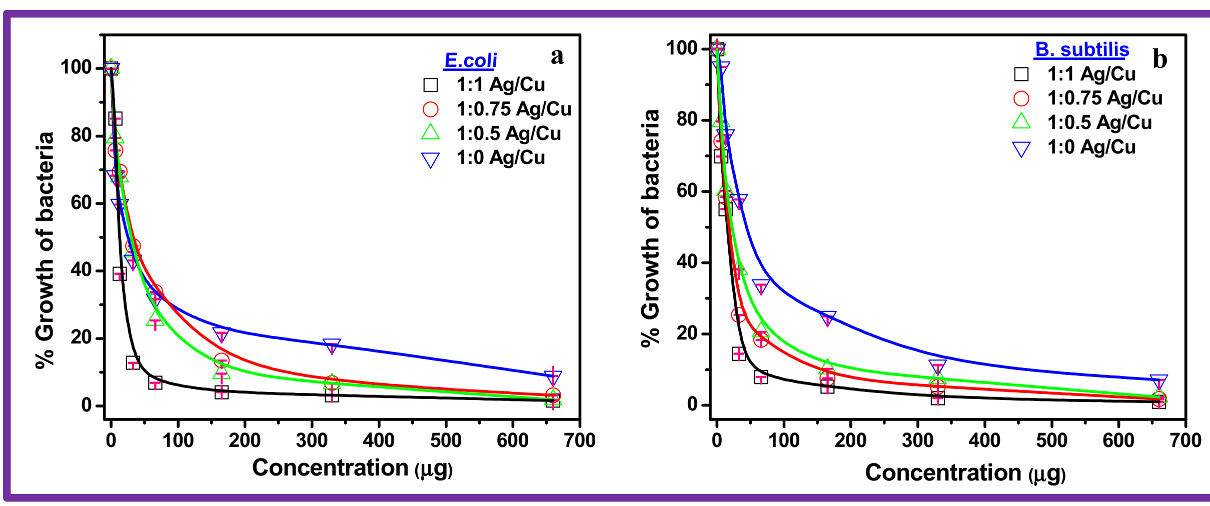

Fig. 7. Plots showing percentage of bacterial growth with respect to concentration of Ag/Cu monoliths with different molar ratios against gram negative (*E. coli*) and gram positive (*B. subtilis*) bacteria.

Table 2
Antibacterial effect of Ag-Cu bimetallic monoliths against *E. coli* and *B. subtilis* measured by EC_{50}.

Monolith	*E. coli*	*B. subtilis*
Ag/Cu-0	40.85 ± 0.012	46.23 ± 0.1
Ag/Cu-1	38.056 ± 0.034	32.51 ± 0.07
Ag/Cu-2	33.86 ± 0.009	28.33 ± 0.16
Ag/Cu-3	22.87 ± 0.015	23.33 ± 0.09

number of reactant molecules passes through the catalytic cycle beforehand the catalyst gets inactivated.

$$TON = \frac{Number\ of\ reactant\ molecules}{Number\ of\ catalyst\ molecules} \times yield$$

$$TOF = \frac{TON}{Time}$$

TOF is characteristically defined as the total number of reactant molecules converted into desired product per unit time (s) per gram of Ag-Cu monoliths. Table 3 shows the catalytic efficiency with TOF of Ag-Cu monoliths.

3.3.2. Thermodynamic study

Thermodynamic parameters (like activation energy) for catalytic reduction of 4-NP for all monoliths, were evaluated at various temperatures (283 K, 288 K, 293 K and 298 K). Non- linear increase in rate constant was observed by mean of increase in tem-

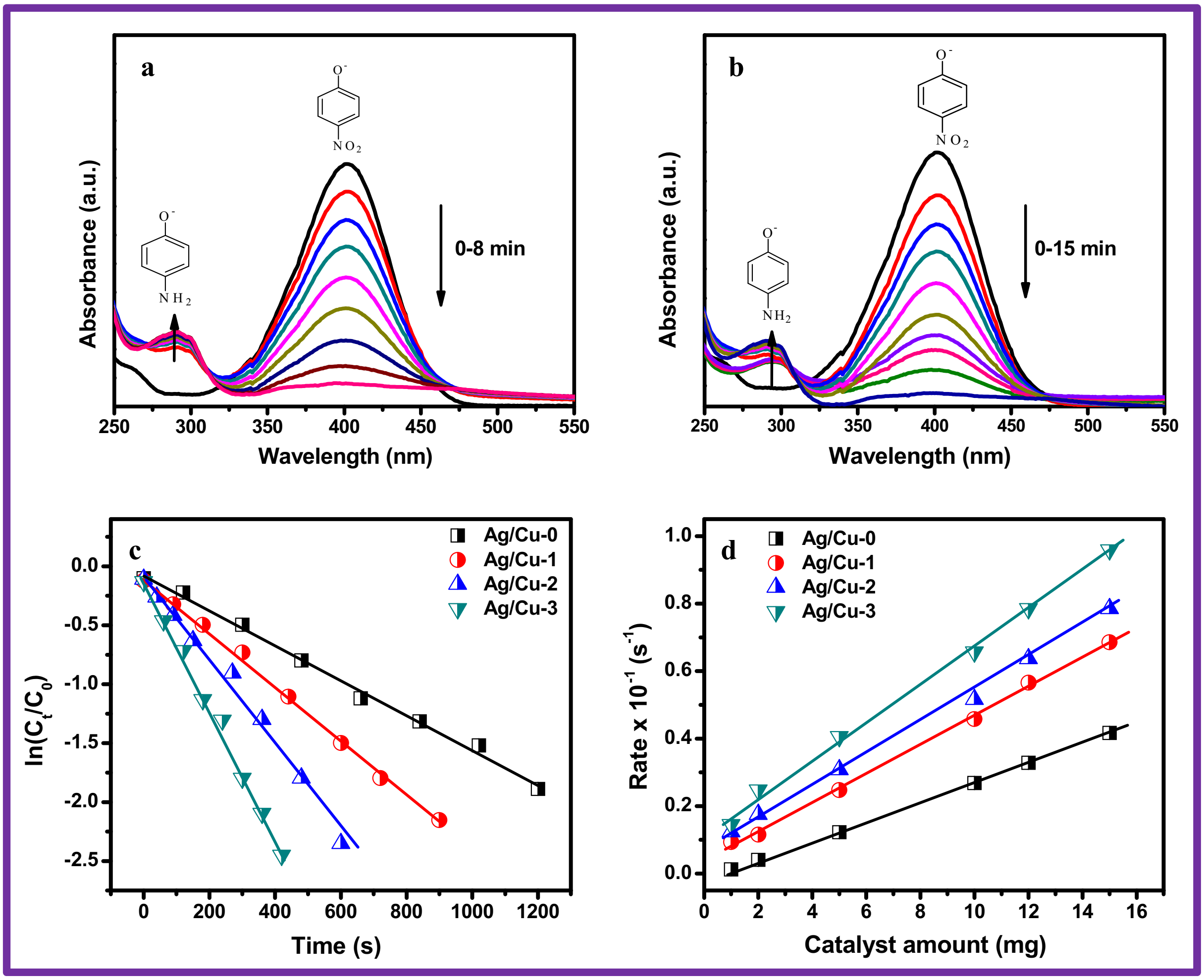

Fig. 8. UV–Visible spectra showing evolution of 4-AP for (a) Ag/Cu-3 and (b) Ag/Cu-1 bimetallic monolith; plot showing kinetic study (c) $\ln(C_t/C_0)$ vs. time and (d) rate vs. catalyst amount.

Table 3
The rate constants and corresponding TOF values for the catalytic reduction of 4-NP over different Ag-Cu monoliths.

Monolith	S_{BET} ($m^2\ g^{-1}$)	Time (min)	Rate constant (k, $10^{-2}\ s^{-1}$)	TOF (h^{-1})
Ag/Cu-0	14 ± 5	20	0.46	37.5
Ag/Cu-1	39 ± 5	15	2	52.1
Ag/Cu-2	52 ± 5	10	3.7	80.6
Ag/Cu-3	110 ± 5	8	5.5	116.6

perature (Fig. 10a). Activation energy (E_g) of 4-NP reduction reaction was calculated using Arrhenius equation:

$$\ln\ k = -\frac{E_a}{RT} + \ln\ A \quad (2)$$

where k is rate constant at temperature (T), A is absorbance and R is the molar gas constant. The calculated E_a using Ag-Cu bimetallic monolith as heterogeneous catalyst was found to be 82.7 kJ mol^{-1}.

Thermodynamic parameters like enthalpy change (ΔH) and entropy change (ΔS) were also calculated (Table 4) and the reaction was found to be endothermic which is not related to the catalyst used because measured ΔH values were more than zero.

In comparison with other published works, the as synthesized Ag-Cu bimetallic monoliths showed a high rate of conversion of 4-NP to 4-AP (Table 5). Therefore, it could be considered that Ag-Cu bimetallic monoliths could be utilized as an additional catalyst for the catalytic reduction of 4-NP to 4-AP at room temperature.

3.3.3. Reusability of catalyst

Reusability of a catalyst is an important aspect in decrease the production cost of catalyst. Here, reusability of the Ag-Cu bimetallic monoliths were examined in consecutive catalytic cycles, was reused at least 8 times for 4-NP reduction reaction (Fig. 10b). There is no permanent adsorption of 4-NP occurs over the surface of Ag-Cu bimetallic monoliths due to which it can directly be separated by simple filtration and centrifugation. The percentage reduction was maintained over 60–75% after 8 cycles.

4. Conclusion

Mesoporous bimetallic Ag-Cu monoliths with a small amount of micropores were synthesized via nanocasting method. Of interest is that the synthesized monoliths showed effective bactericidal against *E. coli* and *B. Subtilis* and calculated EC_{50} using Ag/Cu-3 bimetallic monolith after 24 h of incubation was found to be

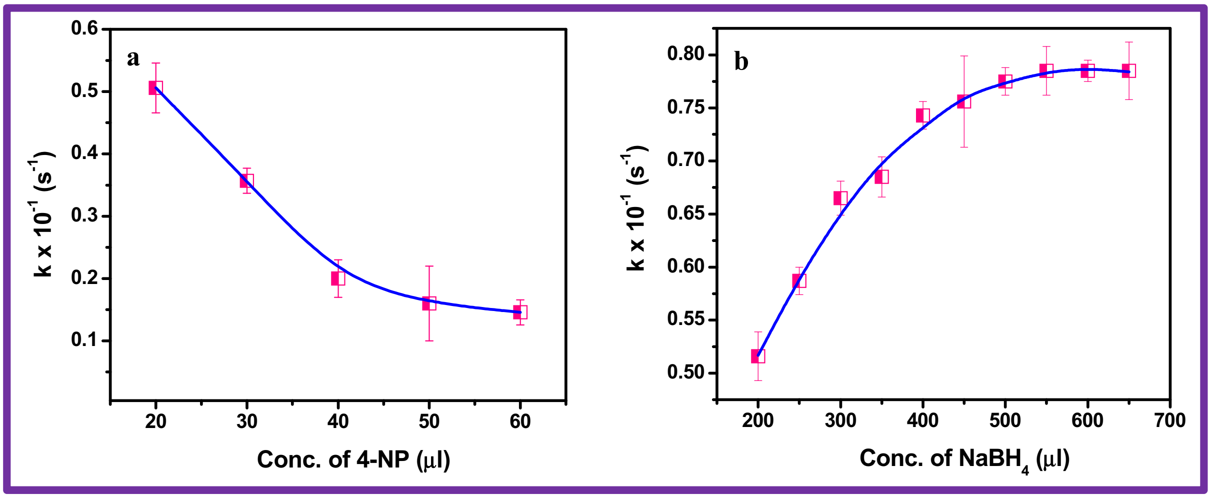

Fig. 9. Effect of concentration of (a) 4-NP and (b) $NaBH_4$ on rate of reduction reaction using Ag/Cu-3 monolith as catalyst [condition: dose of catalyst – 0.2g/L; agitation speed – 200 rpm; temperature – 25 °C].

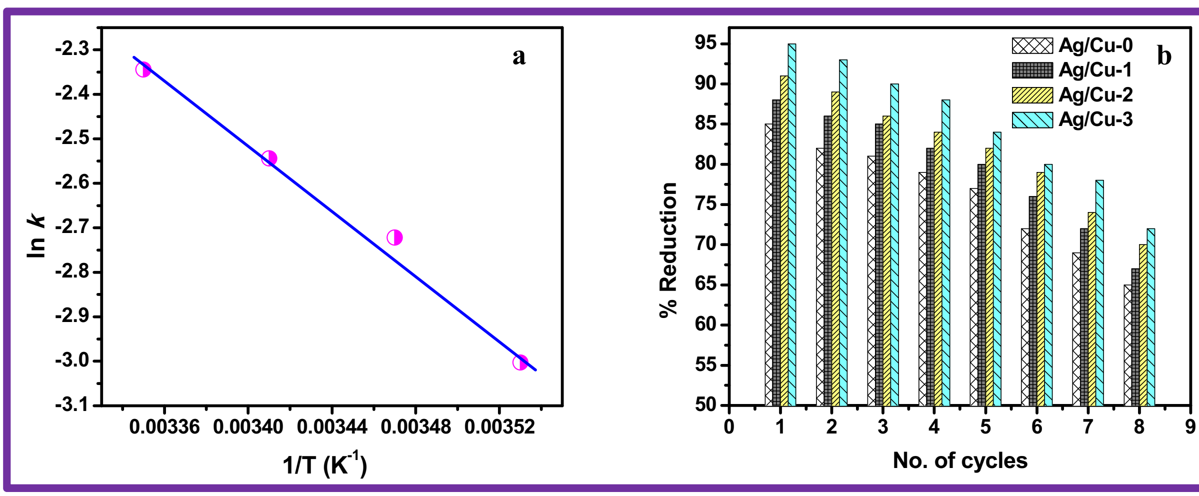

Fig. 10. Plots of (a) ln k vs. 1/T to define the thermodynamic parameters for Ag/Cu-3 monolith and (b) percentage reduction vs. no. of cycles to check the reusability of the catalyst.

Table 4
Temperature-dependent reduction rate of 4-NP reduction using Ag/Cu-3 monoliths.

Temperature (K)	k (s^{-1}) × 10^{-2}	E_a (kJ mol^{-1})	ΔH (kJ mol^{-1})	ΔS (J mol^{-1} K^{-1})
283	2.4	82.7	11.2	45.12
288	3.6			
293	4.0			
298	4.9			

Table 5
A comparative analysis for the catalytic reduction reaction of the different catalysts.

Catalyst	Catalyst amount (g/L)	4-NP (M)	$NaBH_4$ (M)	Rate (s^{-1})	Percentage rate of reduction	Reference
Cu-Ag/CA	–	1×10^{-2}	0.015	0.44×10^{-2}	88	[35]
Pt_3Au1-PDA/RGO	2	1×10^{-2}	0.1	9.58×10^{-3}	Σ100	[36]
Au/g-C3N4	0.2	1×10^{-2}	0.03	0.61×10^{-3}	95	[37]
AuNPs/GNs	25	1×10^{-2}	0.01	1.44×10^{-2}	Σ80	[38]
Ag/Cu-3	0.2	1×10^{-2}	0.1	5.23×10^{-2}	96	Current study

22.87 ± 0.015 and 23.33 ± 0.09 respectively. Furthermore, kinetic catalytic reduction reactions of 4-NP in the presence of bimetallic Ag-Cu monolith (with different molar ratio) by $NaBH_4$ were performed. Additionally, kinetic rate constant and activation energy were also evaluated to be 2–5.5 × 10^{-2} (s^{-1}) and 82.7 kJ mol^{-1}. The catalyst efficiency was determined on the basis of TOF and recyclability. The new as-prepared mesoporous bimetallic Ag-Cu catalysts are stable, efficient, easy to prepare, and recyclable and thus have potential for industrial applications.

Acknowledgement

Authors are thankful to DAE-BRNS (Grant No: 34/14/63/2014), Mumbai, India for fellowship and other financial assistance. Authors are also thankful to Thapar University (DST-FIST) for providing instrumental facilities.

References

[1] Y. Du, H. Chen, R. Chen, N. Xu, Synthesis of p-aminophenol from p-nitrophenol over nano-sized nickel catalysts, Appl. Catal. A 277 (2004) 259–264.
[2] Y.-P. Li, H.-B. Cao, C.-M. Liu, Y. Zhang, Electrochemical reduction of nitrobenzene at carbon nanotube electrode, J. Hazard. Mater. 148 (2007) 158–163.
[3] Z.V. Feng, J.L. Lyon, J.S. Croley, R.M. Crooks, D.A.V. Bout, K.J. Stevenson, Synthesis and catalytic evaluation of dendrimer-encapsulated Cu nanoparticles. An undergraduate experiment exploring catalytic nanomaterials, J. Chem. Educ. 86 (2009) 368.
[4] N. Pradhan, A. Pal, T. Pal, Catalytic reduction of aromatic nitro compounds by coinage metal nanoparticles, Langmuir 17 (2001) 1800–1802.
[5] M. Nemanashi, R. Meijboom, Synthesis and characterization of Cu, Ag and Au dendrimer-encapsulated nanoparticles and their application in the reduction of 4-nitrophenol to 4-aminophenol, J. Colloid Interface Sci. 389 (2013) 260–267.
[6] K. Kuroda, T. Ishida, M. Haruta, Reduction of 4-nitrophenol to 4-aminophenol over Au nanoparticles deposited on PMMA, J. Mol. Catal. A: Chem. 298 (2009) 7–11.
[7] M. Sharma, A. Mishra, V. Kumar, S. Basu, Green synthesis of silver nanoparticles with exceptional colloidal stability and its catalytic activity toward nitrophenol reduction, Nano 11 (2016) 1–10.
[8] A. Mehta, M. Sharma, A. Kumar, S. Basu, Gold nanoparticles grafted mesoporous silica: a highly efficient and recyclable heterogeneous catalyst for reduction of 4-nitrophenol, Nano 11 (2016) 1–9.
[9] T.P. Ang, W.S. Chin, Dodecanethiol-protected copper/silver bimetallic nanoclusters and their surface properties, J. Phys. Chem. B 109 (2005) 22228–22236.
[10] J. Zhao, D. Zhang, X. Zhang, Preparation and characterization of copper/silver bimetallic nanowires with core-shell structure, Surf. Interface Anal. 47 (2015) 529–534.
[11] Z. Khan, A.Y. Obaid, Seedless, copper-induced synthesis of stable Ag/Cu bimetallic nanoparticles and their optical properties, RSC Adv. 6 (2016) 29116–29126.
[12] N.N. Kariuki, J. Luo, M.M. Maye, S.A. Hassan, T. Menard, H.R. Naslund, Y. Lin, C. Wang, M.H. Engelhard, C.J. Zhong, Composition-controlled synthesis of bimetallic gold-silver nanoparticles, Langmuir 20 (2004) 11240–11246.
[13] M.S. Bakshi, F. Possmayer, N.O. Petersen, Simultaneous synthesis of Au and Cu nanoparticles in pseudo-core-shell type arrangement facilitated by DMPG and 12-6-12 capping agents, Chem. Mater. 19 (2007) 1257–1266.
[14] L. Rivas, S. Sanchez-Cortes, J.V. García-Ramos, G. Morcillo, Mixed silver/gold colloids: a study of their formation, morphology, and surface-enhanced Raman activity, Langmuir 16 (2000) 9722–9728.
[15] K.K. Haldar, S. Kundu, A. Patra, Core-size-dependent catalytic properties of bimetallic Au/Ag core-shell nanoparticles, Appl. Mater. Interfaces 6 (2014) 21946–21953.
[16] I. Najdovski, P.R. Selvakannan, S.K. Bhargava, A.P. O'Mullane, Formation of nanostructured porous Cu-Au surfaces: the influence of cationic sites on (electro)-catalysis, Nanoscale 4 (2012) 6298–6306.
[17] K.-Y. Yoon, J. Hoon Byeon, J.-H. Park, J. Hwang, Susceptibility constants of Escherichia coli and Bacillus subtilis to silver and copper nanoparticles, Sci. Total Environ. 373 (2007) 572–575.
[18] M. Valodkar, S. Modi, A. Pal, S. Thakore, Synthesis and anti-bacterial activity of Cu, Ag and Cu–Ag alloy nanoparticles: a green approach, Mater. Res. Bull. 46 (2011) 384–389.
[19] K.-T. Chen, D. Ray, Y.-H. Peng, Y.-C. Hsu, Preparation of Cu–Ag core–shell particles with their anti-oxidation and antibacterial properties, Curr. Appl. Phys. 13 (2013) 1496–1501.
[20] C. Rousse, J. Josse, V. Mancier, S. Levi, S.C. Gangloff, P. Fricoteaux, Synthesis of copper–silver bimetallic nanopowders for a biomedical approach; study of their antibacterial properties, RSC Adv. 6 (2016) 50933–50940.
[21] D. Wang, Q. Peng, Y. Li, Nanocrystalline intermetallics and alloys, Nano Res. 3 (2010) 574–580.
[22] R. Hao, R. Xing, Z. Xu, Y. Hou, S. Gao, S. Sun, Synthesis, functionalization, and biomedical applications of multifunctional magnetic nanoparticles, Adv. Mater. 22 (2010) 2729–2742.
[23] A. Taguchi, F. Schuth, Ordered mesoporous materials in catalysis, Micropor. Mesopor. Mater. 77 (2005) 1–45.
[24] M. Sharma, A. Mishra, A. Mehta, D. Choudhury, S. Basu, Enhanced catalytic and antibacterial activity of nanocasted mesoporous silver monoliths: kinetic and thermodynamic studies, J. Sol-Gel. Sci. Technol. 81 (2016) 704–710.
[25] N. Pradhan, A. Pal, T. Pal, Silver nanoparticle catalyzed reduction of aromatic nitro compounds, Colloids Surf., A 196 (2002) 247–257.
[26] H.R. Nikabadi, N. Shahtahmasebi, M.R. Rokn-Abadi, M. Karimipour, M.M.B. Mohagheghi, Structural verification and optical characterization of SiO_2-Au-Cu_2O nanoparticles, Bull. Mater. Sci. 37 (2014) 527–532.
[27] A.A. Dubale, C.-J. Pan, A.G. Tamirat, H.-M. Chen, W.-N. Su, C.-H. Chen, J. Rick, D. W. Ayele, B.A. Aragaw, J.-F. Lee, Y.-W. Yang, B.-J. Hwang, Heterostructured Cu_2O/CuO decorated with nickel as a highly efficient photocathode for photoelectrochemical water reduction, J. Mater. Chem. A 3 (2015) 12482–12499.
[28] W. Wu, M. Lei, S. Yang, L. Zhou, L. Liu, X. Xiao, C. Jiang, V.A.L. Roy, A one-pot route to the synthesis of alloyed Cu/Ag bimetallic nanoparticles with different mass ratios for catalytic reduction of 4-nitrophenol, J. Mater. Chem. A 3 (2015) 3450–3455.
[29] F. Zaera, Nanostructured materials for applications in heterogeneous catalysis, Chem. Soc. Rev. 42 (2013) 2746–2762.
[30] Y. Mei, Y. Lu, F. Polzer, M. Ballauff, M. Drechsler, Catalytic activity of palladium nanoparticles encapsulated in spherical polyelectrolyte brushes and core−shell microgels, Chem. Mater. 19 (2007) 1062–1069.
[31] Y. Mei, G. Sharma, Y. Lu, M. Ballauff, M. Drechsler, T. Irrgang, R. Kempe, High catalytic activity of platinum nanoparticles immobilized on spherical polyelectrolyte brushes, Langmuir 21 (2005) 12229–12234.
[32] S. Wunder, F. Polzer, Y. Lu, Y. Mei, M. Ballauff, Kinetic analysis of catalytic reduction of 4-nitrophenol by metallic nanoparticles immobilized in spherical polyelectrolyte brushes, J. Phys. Chem. C 114 (2010) 8814–8820.
[33] S. Saha, A. Pal, S. Kundu, S. Basu, T. Pal, Photochemical green synthesis of calcium-alginate-stabilized Ag and Au nanoparticles and their catalytic application to 4-nitrophenol reduction, Langmuir 26 (2010) 2885–2893.
[34] H. Wu, Z. Liu, X. Wang, B. Zhao, J. Zhang, C. Li, Preparation of hollow capsule-stabilized gold nanoparticles through the encapsulation of the dendrimer, J. Colloid Interface Sci. 302 (2006) 142–148.
[35] F.U. Khan Asimullah, S.B. Khan, T. Kamal, A.M. Asiri, I.U. Khan, K. Akhtar, Novel combination of zero-valent Cu and Ag nanoparticles @ cellulose acetate nanocomposite for the reduction of 4-nitro phenol, Int. J. Biol. Macromol. 102 (2017) 868–877.
[36] W. Ye, J. Yu, Y. Zhou, D. Gao, D. Wang, C. Wang, D. Xue, Green synthesis of Pt–Au dendrimer-like nanoparticles supported on polydopamine-functionalized graphene and their high performance toward 4-nitrophenol reduction, Appl. Catal. B 181 (2016) 371–378.
[37] Y.S. Fu, T. Huang, B.Q. Jia, J.W. Zhu, X. Wang, Reduction of nitrophenols to aminophenols under concerted catalysis by Au/g-C_3N_4 contact system, Appl. Catal. B 202 (2017) 430–437.
[38] X. Chen, Z. Cai, X. Chen, M. Oyama, AuPd bimetallic nanoparticles decorated on graphene nanosheets: their green synthesis, growth mechanism and high catalytic ability in 4-nitrophenol reduction, J. Mater. Chem. A 2 (2014) 5668–5674.